

# A time-series *VI* study of the variable stars of the globular cluster NGC 6397\*

J. A. Ahumada\*

*Observatorio Astronómico, Universidad Nacional de Córdoba, Laprida 854, X5000BGR, Córdoba, Argentina*

A. Arellano Ferro

*Universidad Nacional Autónoma de México, Instituto de Astronomía, AP 70-264, CDMX 04510, México*

I. H. Bustos Fierro

*Observatorio Astronómico, Universidad Nacional de Córdoba, Laprida 854, X5000BGR, Córdoba, Argentina*

C. Lázaro

*Departamento de Astrofísica, Universidad de La Laguna, E-38206 La Laguna, Tenerife, Spain, and  
Instituto de Astrofísica de Canarias (IAC), E-38205 La Laguna, Tenerife, Spain*

M. A. Yopez

*Universidad Nacional Autónoma de México, Instituto de Astronomía, AP 70-264, CDMX 04510, México*

K. P. Schröder

*Universidad de Guanajuato, Departamento de Astronomía, Guanajuato 36000, México*

J. H. Calderón

*Observatorio Astronómico, Universidad Nacional de Córdoba, Laprida 854, X5000BGR, Córdoba, Argentina, and  
Consejo Nacional de Investigaciones Científicas y Técnicas (CONICET), Buenos Aires, Argentina*

---

## Abstract

We present a new time-series *VI* CCD photometry of the globular cluster NGC 6397, from which we obtained and analysed the light curves of 35 variables carefully identified in the cluster field. We assessed the membership of the variables with an astrometric analysis based on *Gaia* DR2 data. The cluster colour-magnitude diagram was differentially dereddened and cleaned of non members, which allowed us to fit isochrones for  $[\text{Fe}/\text{H}] = -2.0$  dex in the range 13.0–13.5 Gyr, for a mean reddening  $E(B - V) = 0.19$ , and a distance of 2.5 kpc. This distance was confirmed using the period-luminosity relation for the cluster's five SX Phoenicis variables (V10, V11, V15, V21, and V23) present among its blue stragglers, yielding  $2.24 \pm 0.13$  kpc. We also modelled the light curves of four eclipsing binaries (V4, V5, V7, and V8), and gave the parameters of the systems; the contact binaries V7 and V8 have distances consistent with that of the cluster. NGC 6397 appears to harbour no RR Lyrae stars, being its horizontal branch remarkably blue, much like that of its analogous cluster, M10. To match the blue tail of the horizontal branch population, models of  $0.64\text{--}0.66 M_{\odot}$  with mass loss at the RGB are required, indicating rather thin shell masses for the HB stars.

*Keywords:* globular clusters: individual (NGC 6397), binaries: eclipsing, Stars: variables: RR Lyrae, blue stragglers, horizontal-branch

---

## 1. Introduction

Galactic globular clusters, one of the most luminous remnants of the formation epoch of our Galaxy, play a central role in several areas of astronomy. Being its stellar components at the same distance and of similar age, the stellar mass distribution allows the comparison of stars in different evolutionary stages, they are tracers of the structure of the galactic halo, they are good laboratories for the study of stellar dynamical processes, they give key information on the early evolution of our Galaxy and other galaxies, and their ages and compositions provide severe constraints on cosmological models. Much investigation has been focused on the understanding of the variable stars that globular clusters typically harbour, in particular—but not only—the RR Lyrae stars, from the observational and theoretical points of view. These stars can be used to derive independent estimates of several properties for individual stars and for the cluster as a whole.

In a series of works, mostly summarized in Arellano Ferro et al. (2017), hereafter AF17, our group has been employing CCD time series photometry of globular clusters to update their variable star census and to obtain independent and homogeneous estimates of their metallicity and distance.

In this paper we analyse time-series observations of NGC 6397 (C1736–536 in the IAU nomenclature), located at  $\alpha = 17^{\text{h}} 40^{\text{m}} 42^{\text{s}}.09$ ,  $\delta = -53^{\circ} 40' 27''.6$  (J2000),  $l = 338^{\circ}.17$ ,  $b = -11^{\circ}.96$ . With  $[\text{Fe}/\text{H}] \approx -2.0$  (Carretta et al., 2009), it is one of the most metal-poor globular clusters. Its high King central concentration parameter ( $c = 2.50$ , Trager et al. 1995) indicates that it is one of the Milky Way clusters that would have suffered core collapse (Djorgovski & King, 1986). Its foreground reddening  $E(B - V)$  is 0.16–0.19 mag according to the galactic dust calibrations of Schlafly & Finkbeiner (2011) and Schlegel et al. (1998), and it has an estimated age of about 13.4 Gyr (Gratton et al., 2003), being thus one of the oldest Galactic

globular clusters. However, a recent determination by Correnti et al. (2018), that uses IR WFC3@HST data and isochrone fittings, brings the cluster to  $12.6 \pm 0.7$  Gyr, an age akin to that of most similar systems. At  $\sim 2.5$  kpc (Gratton et al., 2003), this cluster is the second nearest to the Sun, after NGC 6121 (M4).

The *Catalogue of Variable Stars in Globular Clusters*<sup>1</sup> (CVSGC, Clement et al. 2001) lists 36 variables in the field of the cluster, of which only one or perhaps two are of RR Lyrae type. Variables V1 (V639 Ara) and V2 (V825 Ara) were discovered by Bailey (1902). Star V3, an RRab variable, was mentioned by H. H. Swope in unpublished correspondence with H. B. Sawyer, who assigned the number three in her 2nd catalogue (Sawyer, 1955); V3 is considered to be a field star and is designated as V826 Ara in the *Moscow General Catalogue of Variable Stars*<sup>2</sup> (GCVS, Samus et al. 2017). Stars V4 to 11 were announced by Kaluzny (1997), although V10 had already been identified as the blue straggler BS#11 by Lauzeral et al. (1992). Stars V10 and V11 are pulsating variables of the SX Phoenicis type. Variables 12–24 were identified by Kaluzny & Thompson (2003). Stars V15, V21, and V23 are SX Phe variables; stars V22 and V23 are also listed by Lauzeral et al. (1992) as blue stragglers BS#8 and BS#16. Star V22, however, is listed in the CVSGC as a field RRc? variable. The ellipsoidal variable V16 is the optical component of the millisecond pulsar J1740–534; based on radial velocity determinations, Kaluzny & Thompson (2003) and Kaluzny et al. (2008) conclude that it is a cluster member. Finally, Kaluzny et al. (2006) announced stars V25 to 36, among them one irregular variable (V26), two eclipsing binaries (V30 and V32), two optical counterparts of cataclismic variables (V33 and V34), and the rest variable stars of possibly assorted although unconfirmed types.

A post-core-collapse, dynamically evolved globular cluster, NGC 6397 boasts of harbouring about two dozen blue stragglers near the cluster centre, revealed by ground-based CCD photometry (Aurriere et al., 1990; Lauzeral et al., 1992), as well as at least 79 X-ray sources detected by NASA’s Chandra X-ray telescope within its half-mass radius (Grindlay et al., 2001). Based on HST data, Cohn et al. (2010) published optical identifications for the 79 X-ray sources, among them stars V7, V12, V13,

---

\*Based on observations at Estación Astrofísica de Bosque Alegre, Argentina, and at Las Campanas Observatory, Chile

\*Corresponding author

*Email addresses:* javier.ahumada@unc.edu.ar (J. A. Ahumada), armando@astro.unam.mx (A. Arellano Ferro), ivan.bustos.fierro@unc.edu.ar (I. H. Bustos Fierro), clh@iac.es (C. Lázaro), myepe@astro.unam.mx (M. A. Yopez), astrop85@gmail.com (K. P. Schröder), jehumcal@gmail.com (J. H. Calderón)

---

<sup>1</sup><http://www.astro.utoronto.ca/~cclement/read.html>

<sup>2</sup><http://www.sai.msu.su/gcvs/gcvs/vartype.htm>

V14, V16, V17, V20, V24, V26, V30, V31, V33, V34, V35, and V36. In particular, stars V12 and V13 are the optical counterparts to cataclismic variables CV1 and CV6 of Grindlay et al. (2001), and stars V33 and 34 are the optical counterparts to CV3 and CV2, in which Shara et al. (2005) found dwarf nova-like eruptions.

For the sake of completeness, it is also worth mentioning these more recent developments. First, the search for planetary transits of Nascimbeni et al. (2012), who identified 12 new variables among low-main-sequence stars, all of them considered to belong to the field, based on the proper motions and positions in the colour-magnitude diagram. Second, the photometric survey by Martinazzi et al. (2017) who, also among the stars of the lower main sequence of NGC 6397, found 412 suspected variables. And third, the report by Marcano et al. (2021) of optical modulations in the companion to the X-ray source U18, which gives support to the interpretation that it is the second “redback” millisecond pulsar known in the cluster.

In this paper we present a new time-series photometry of NGC 6397. By analysing the light curves of the cluster variables, we want to obtain information on the variable stars and their parent system. This is the layout of the paper. In § 2 we present our observations and describe the DIA photometric process; § 3 deals with the colour-magnitude diagram, including the description of the *Gaia* DR2 method employed to select the cluster members, and the matching of isochrones; in § 4 we give the accurate identification and membership of all the cluster variables; § 5 is devoted to the modelling of four eclipsing binaries in the field of the cluster; in § 6 we derive the distance to the cluster using several methods; in § 7 we discuss the structure of the cluster horizontal branch, and present its modelling using the Eggleton codes with mass loss during the red giant stage; finally, in § 8 we give an account of the results of the work.

## 2. Data and reductions

### 2.1. Observations

The observations were performed in two sites. First, the Bosque Alegre Astrophysical Station of the Córdoba Observatory, National University of Córdoba, Argentina, whose 1.54-metre telescope was used on 19 nights between June 3, 2017 and August 5, 2018. We used a camera Alta F16M with a

detector KAF-16803 of  $4096 \times 4096$  square 9-micron pixels, binned  $2 \times 2$ , with a scale of 0.496 arcsec/pix after binning. Due to coma, the binned Bosque Alegre images were trimmed to  $1160 \times 1160$  pixels, for a useful field of view (FoV) of  $9.7' \times 9.7'$ . Second, Las Campanas Observatory, Chile, whose 1.0-metre Swope Telescope was used on the night of June 28, 2018, with the CCD E2V 231-84 of  $4096 \times 4112$  pixels also binned  $2 \times 2$ ; the scale is 0.435 arcsec/pixel after binning, and the FoV is  $15.0' \times 14.9'$ . A total of 748 (*V*) and 737 (*I*) images were acquired along the 20 nights. The log of observations is in Table 1, where the dates, number of frames, exposure times, and average nightly seeing are listed.

### 2.2. Difference image analysis

To carry out high-precision photometry for all the point sources in our collection of images of NGC 6397, we applied the recognised technique of difference image analysis (DIA). As in previous papers, we employed the DanDIA<sup>3</sup> pipeline for the data reduction process (Bramich, 2008; Bramich et al., 2013). The Bosque Alegre and Las Campanas images were reduced independently. Reference images for the *V* and *I* filters, and for each observatory, were built by stacking the best-quality images in our collection. Sequences of difference images in each filter were then built by subtracting the respective convolved reference image from the rest of the series. Differential fluxes for each star detected in the reference image were measured on each difference image. Finally, light curves for each star were constructed from the series of differential images, by calculating the total flux  $f_{\text{tot}}(t)$  at each epoch  $t$  from:

$$f_{\text{tot}}(t) = f_{\text{ref}} + \frac{f_{\text{diff}}(t)}{p(t)}, \quad (1)$$

where  $f_{\text{ref}}$  is the reference flux,  $f_{\text{diff}}(t)$  is the differential flux, and  $p(t)$  is a photometric scale factor. Conversion to instrumental magnitudes is achieved using:

$$m_{\text{ins}}(t) = 25.0 - 2.5 \log [f_{\text{tot}}(t)], \quad (2)$$

where  $m_{\text{ins}}(t)$  is the instrumental magnitude of the star at time  $t$ . All fluxes are in  $\text{ADU s}^{-1}$ , and uncertainties are propagated as usual. The procedure is described, with details and caveats, by Bramich et al. (2011).

<sup>3</sup>DanDIA is built from the DanIDL library of IDL routines available at <http://www.danidl.co.uk>.

Table 1: Distribution of observations of NGC 6397

Date	$N_V$	$t_V$ [s]	$N_I$	$t_I$ [s]	Seeing ["]
20170603	9	400	11	200	1.5
20170616	6	400	7	200	2.6
20170630	8	400	9	200	1.3
20170701	12	400	12	200	1.8
20170728	12	400	12	200	1.8
20170818	9	400	11	200	2.4
20170819	18	400	18	200	1.8
20170820	24	90,160,300,400	23	50,60,120,200	1.4
20170826	5	120	6	60	1.4
20170901	22	120	25	60	1.9
20170915	27	120	26	60	1.8
20170922	37	120	37	60	1.3
20171006	17	120	6	60	1.7
20180518	63	40,120	58	20,60	1.6
20180519	75	40,200	77	20,100	1.5
20180623	56	60	55	30	2.2
20180628*	193	5,10	193	1,3	1.3
20180803	60	60	60	30	1.3
20180804	55	60	52	30	1.2
20180805	40	60	39	30	1.2

**Notes.** Columns  $N_V$  and  $N_I$  give the number of images taken with the  $V$  and  $I$  filters. Columns  $t_V$  and  $t_I$  provide the exposure time, or range of exposure times. The average seeing is listed in the last column. Observations are from Bosque Alegre Astrophysical Station, except the asterisked night.

### 2.3. Photometric calibrations

To correct for possible systematic errors, we applied the methodology developed by Bramich & Freudling (2012) to solve for the magnitude offsets to be subtracted from each photometric measurement made on a given image. This is a first-order correction to the systematic uncertainty introduced into the photometry of an image, due to an error in the fitted value of the scale factor  $p$  (Equation 1). In the present case, the systematic error corrections were found to be negligible, always smaller than 1 mmag, except in the case of the  $I$  photometry from Las Campanas, where a correction of 6 mmag was calculated and applied for stars brighter than the 15th magnitude.

### 2.4. Transformation to the standard system

Standard stars in the field of NGC 6397 are included in the online collection of Stetson (2000),<sup>4</sup> which were used to transform our instrumental  $vi$  magnitudes into the Johnson-Kron-Cousins  $VI$  system. The mild colour dependences of the standard  $minus$  instrumental magnitudes are shown in Fig. 1 for the observations from Bosque Alegre and Las Campanas. The transformation equations are given in the figure itself. However, given the non-significant colour dependence for the Bosque Alegre data, we opted to transform them to the standard system using the linear relations:  $V = (0.980 \pm 0.004) \times v - (2.012 \pm 0.082)$  and  $I = (0.985 \pm 0.004) \times i - (2.926 \pm 0.068)$ , since they provide a good agreement with Las Campanas observations, of better spatial resolution.

## 3. The colour-magnitude diagram

### 3.1. Cluster stellar membership

We applied the method of Bustos Fierro & Calderón (2019) to identify probable members in the field of the cluster. It uses the high quality astrometric data available in *Gaia* DR2, implementing the Balanced Iterative Reducing and Clustering using Hierarchies (BIRCH) algorithm (Zhang et al., 1996) in a four-dimensional space of physical parameters—positions and proper motions—that detects groups of stars in the 4D-space. In this way we extracted 31,047 *Gaia* stellar sources

that are likely cluster members, from a much larger sample of 472,304 stars within 60 arcmin around the cluster. A total of 17,482 stars are in the field of our Las Campanas images, of which 12,971 are considered members. Figure 2 shows the Vector-Point Diagram (VPD) of cluster and field stars, and the corresponding *Gaia* colour-magnitude diagram.

### 3.2. Cluster reddening

NGC 6397 belongs to a group of globular clusters located toward the centre of the Milky Way; hence, it is affected by interstellar reddening of a patchy nature. To differentially deredden our photometry, we employed the differential reddening grid calculated by Alonso-García et al. (2012), that covers nearly the whole field of our images from the Swope telescope. The resolution of the grid is  $5.4''$  ( $0^\circ 36'$ ) in RA and  $3.6''$  in DEC. The procedure to deredden each star starts by first averaging the four neighbouring differential reddening values given in the grid, and then adding a mean overall reddening. The mean value of  $E(B - V)$  suggested by Alonso-García et al. (2012) for NGC 6397 is 0.18. The Galactic dust distribution and the calibrations of Schlafly & Finkbeiner (2011) and Schlegel et al. (1998) suggest values of 0.166 and  $0.188 \pm 0.003$ , respectively. In Fig. 3 we show the CMD before (left panel) and after (right panel) the reddening correction and membership cleaning. In the latter we adopted  $E(B - V) = 0.19$  and a distance of 2.5 kpc, to place the two isochrones for 13.0 and 13.5 Gyr. To deredden the colour ( $V - I$ ) we employed the ratio  $E(V - I)/E(B - V) = 1.259$ . Although differential reddening is mild across the NGC 6397 area, a sharper distribution of stars is noticeable after this correction.

### 3.3. Isochrones and ZAHB fitting

The colour-magnitude diagram (CMD) of NGC 6397, built with data from the Swope telescope (the better quality data) is shown in Fig. 3. In the left panel the member and non-member stars are represented by black and light blue points. In the right panel we present the CMD after the non-members have been removed, and the member stars have been subjected to the differential reddening correction (§ 3.2). The CMD diagram appears very clean, which enabled a proper matching of isochrones and ZAHB models. These best fitting models were taken from the grid of the Victoria-Regina models of VandenBerg

<sup>4</sup><http://www3.cadc-ccda.hia-ihp.nrc-cnrc.gc.ca/community/STETSON/standards>

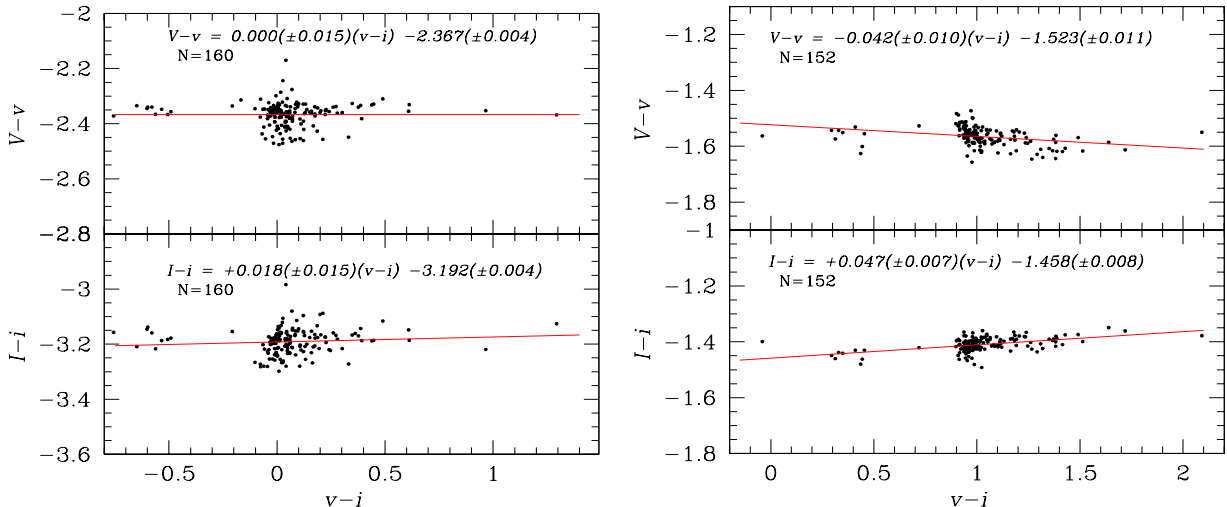


Figure 1: Colour dependence of the transformations for the  $V$  and  $I$  filters between the instrumental and the standard photometric systems. The *left* and *right* panels correspond to the transformations for the observations in Bosque Alegre and Las Campanas, respectively. We employed a set of standard stars of Stetson (2000) present in the field of NGC 6397.

et al. (2014) for  $[\text{Fe}/\text{H}] = -2.0$ ,  $Y = 0.25$ , and  $[\alpha/\text{Fe}] = +0.4$ , and ages of 13.0 and 13.5 Gyr. The isochrones match very well the stellar unreddened distribution for a distance of 2.5 kpc and  $E(B - V) = 0.19$ . It is pertinent to note here that Brown et al. (2018) recently derived, from the  $V$  luminosity at the main-sequence turnoff, an absolute age of  $13.4 \pm 1.2$  Gyr for the cluster.

In the CMD it is evident a very blue horizontal branch void of any RR Lyrae stars. The only two RR Lyrae known in the field of the cluster (V3 and V22) are clearly non-members and background objects, as they appear in the blue straggler area, near the turnoff. The structure of the HB will be discussed in § 7.

#### 4. Variable stars in the field of NGC 6397

The 36 stars catalogued in the CVSGC (Clement et al., 2001), their coordinates and *Gaia* DR2 identifications (when available), and their membership as estimated in this paper, are listed in Table 2. Among them, only V1 and V3 appear flagged as variables in *Gaia* DR2. Finding charts for all variables, except V1, are in Fig. 4.

Several of these stars, such as V12, 13, 14, 33–36, are in the observed field, but are too faint or too near a bright companion to be properly detected or measured in our data. Besides, stars V2, 5, 6, and 9 are outside the trimmed Bosque Alegre field,

i.e., they were observed during only one night at Las Campanas (cf. Table 1); in that night, V2 and V6 did not show any variations. We shall therefore limit our light-curve analysis to those stars—listed in Table 3—of variability clearly detected with our photometry. In all cases we attempted a new determination of the period based on our data, using the string-length method (Dworetzky, 1983). However, a trial and error approach showed that, in some cases, the light curve was better phased with the period given in the CVSGC. In Table 4 we report the  $V$  and  $I$  time-series photometry for all variables in our field of view; the full table, which also includes the parameters of Equation 1 computed by DanDIA, is published only in electronic format. Individual variables are discussed next, and the light curves are shown in Figs. 5 and 6.

##### 4.1. RR Lyrae stars

**V3.** This is the first RRAb star known in the NGC 6397 area; however, there is firm evidence that it does not belong to the cluster. This is confirmed by its position in the CMD, near the cluster turnoff.

**V22.** The second RR Lyrae variable present in the cluster area, it also appears in the blue straggler zone of the CMD and was originally identified as one of them by Lauzeral et al. (1992). In the CVSGC the star is listed as a probable double-mode RR Lyrae, but no periods are suggested. While

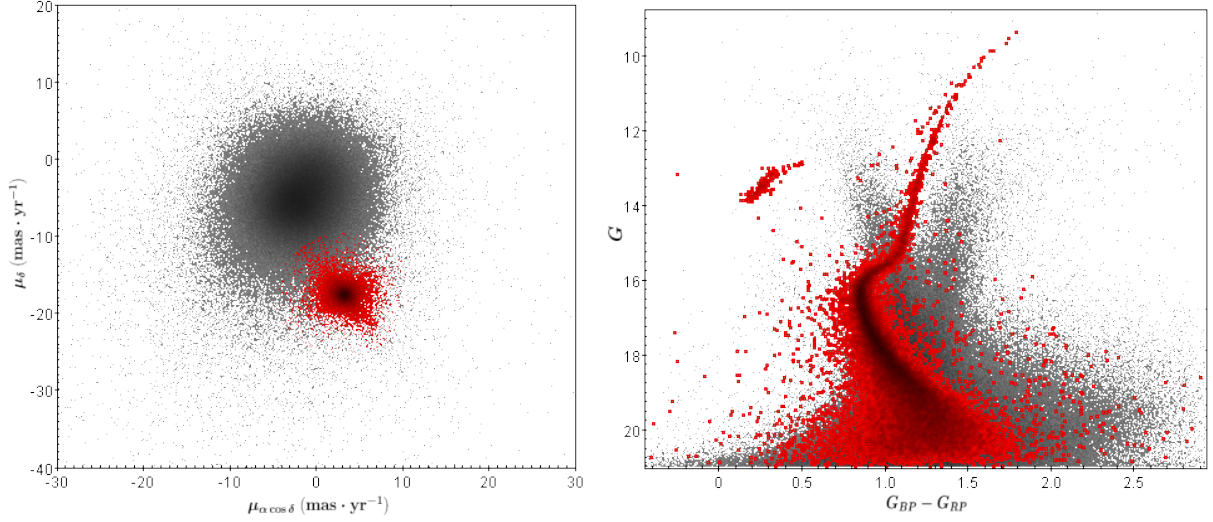


Figure 2: Membership of stars in the NGC 6397 field, based on *Gaia* DR2 data (see § 3.1). The *left* panel shows the Vector-Point Diagram (VPD) for 472,304 stars within 60 arcmin around the cluster. Red dots represent stars considered likely members. The cluster clearly stands out against the vast number of field stars. The *right* panel displays the colour-magnitude diagram in the *Gaia* photometric system.

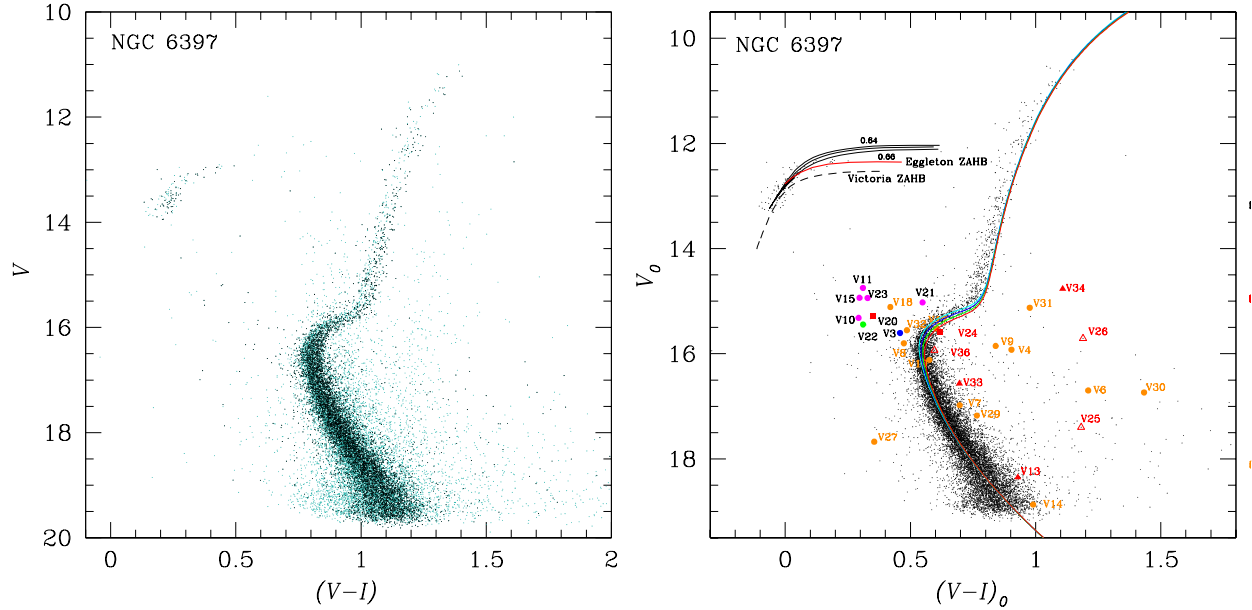


Figure 3: Colour-magnitude diagram of NGC 6397, built from Las Campanas data. The *left* panel shows the observed, reddened stellar distribution. Black and blue dots represent cluster members and field stars respectively, according to the membership analysis of § 3.1. In the *right* panel only cluster members are plotted, after their colours were individually corrected by differential reddening (§ 3.2), and globally shifted an average colour excess  $E(B - V) = 0.19$ . The star sequences appear well matched by four isochrones calculated using the models of Vandenberg et al. (2014), for ages (left to right): 12.0, 12.5, 13.0, and 13.5 Gyr, and  $[\text{Fe}/\text{H}] = -2.0$ ,  $Y = 0.25$ , and  $[\alpha/\text{Fe}] = +0.4$ . The isochrones were located at a distance of 2.5 kpc. At the HB, three continuous black loci, also positioned at 2.5 kpc, show the evolutionary tracks for total masses of 0.64, 0.65, and 0.66  $M_{\odot}$ , calculated as explained in § 7. The resulting ZAHB is shown in red, and for comparison we include, as a dashed line, the ZAHB computed from Vandenberg et al. (2014) models, for the same parameters. The known variables measured in the present study are labelled with different symbols and colours: RRab (*blue*); RRc (*green*); SX Phe (*lilac*);  $\gamma$  Dor-type? and cataclysmic (*red*); contact binaries and ellipsoidal (*orange*).

Table 2: Variable stars in the field of NGC 6397

Variable Id.	Variable Type <sup>a</sup>	V <sup>a</sup> [mag]	RA <sup>b</sup> (J2000.0)	Dec <sup>b</sup> (J2000.0)	<i>Gaia</i> DR2 Source Id.	Memb. <sup>c</sup>
V1	M	13.36	17:41:04.75	-53:32:58.6	5921753573179938304	m?
V2	RV?	12.88	17:40:10.86	-53:47:33.9	5921745812182394496	f
V3	RRab	16.07	17:40:16.98	-53:41:03.6	5921748045565559040	f
V4	EW	16.35	17:41:08.83	-53:42:34.3	5921750072784246400	f
V5	E	18.70	17:41:05.55	-53:33:36.0	5921753573174589440	f
V6	EW	17.16	17:40:53.35	-53:43:39.6	5921744884469398656	f
V7	EW	17.09	17:40:43.93	-53:40:35.5	5921745296766522752	m
V8	EW	16.24	17:40:39.27	-53:38:47.2	5921754161593008384	m
V9	EW	16.25	17:40:02.25	-53:35:45.3	5921755295470448256	f
V10	SX Phe	16.00	17:40:37.55	-53:40:36.5	5921748217344441856	m
V11	SX Phe	15.43	17:40:44.14	-53:40:40.8	5921745296766500224	m
V12 <sup>d</sup>	CV?	17.52	17:40:41.62	-53:40:20.0	...	...
V13	CV?	19.43	17:40:48.94	-53:39:49.5	5921751137936013056	...
V14	E	19.25	17:40:46.50	-53:41:15.7	...	...
V15	SX Phe	15.43	17:40:45.42	-53:40:25.3	5921751172297381120	m
V16	ELL	16.65	17:40:44.63	-53:40:41.9	5921745296766500864	m
V17	ELL?	16.23	17:40:43.82	-53:41:16.6	5921745296766429824	m
V18	E	15.75	17:40:43.64	-53:40:28.0	5921751172301644032	...
V19	E	17.12	17:40:42.85	-53:40:23.8	5921751172301639808	...
V20	$\gamma$ Dor?	15.83	17:40:41.70	-53:40:33.6	5921745296786376320	m
V21	SX Phe	15.47	17:40:41.59	-53:40:23.9	5921745296786384128	...
V22	RRd <sup>c</sup>	16.15	17:40:41.15	-53:40:42.3	5921745296766606336	f
V23	SX Phe	15.52	17:40:39.34	-53:40:47.0	5921748251704126464	...
V24 <sup>e</sup>	$\gamma$ Dor?	16.17	17:40:39.10	-53:40:23.4	...	...
V25	?	17.98	17:41:10.18	-53:39:30.9	5921750652596773888	f
V26	?	16.24	17:40:43.05	-53:38:31.7	5921751305431697920	f
V27	ELL?	18.25	17:41:13.81	-53:41:14.5	5921750244578290816	f
V28	?	15.13	17:41:02.73	-53:39:47.5	5921751000496772224	f
V29	ELL?	19.72	17:40:59.67	-53:40:39.0	5921751034856719488	...
V30	E	17.64	17:40:54.53	-53:40:44.7	5921750931784538112	f
V31	ELL?	15.99	17:40:42.62	-53:40:27.5	5921745296766546176	...
V32	E	16.13	17:40:40.33	-53:41:25.6	5921745262406760960	m
V33	CV?	18.3	17:40:42.71	-53:40:18.7	5921751172296037632	...
V34	CV	16.2	17:40:42.40	-53:40:28.7	5921745296766570368	...
V35 <sup>f</sup>	ELL	18.79	17:40:43.35	-53:41:55.6	...	...
V36	?	16.53	17:40:44.14	-53:42:11.7	5921745155038332032	m

**Notes.**<sup>a</sup>CVSGC (Clement et al., 2001).<sup>b</sup>Coordinates are mostly from *Gaia* DR2, and the rest are from the HST archive image u5dr0401r.<sup>c</sup>This work.<sup>d</sup>Bright *Gaia* source 5921745296786384896 is at 1'' towards the South.<sup>e</sup>*Gaia* source 5921748251704160512 is at 0.7'' towards the NE.<sup>f</sup>Bright *Gaia* source 5921745262406612608 is at 1.3'' towards the SE.



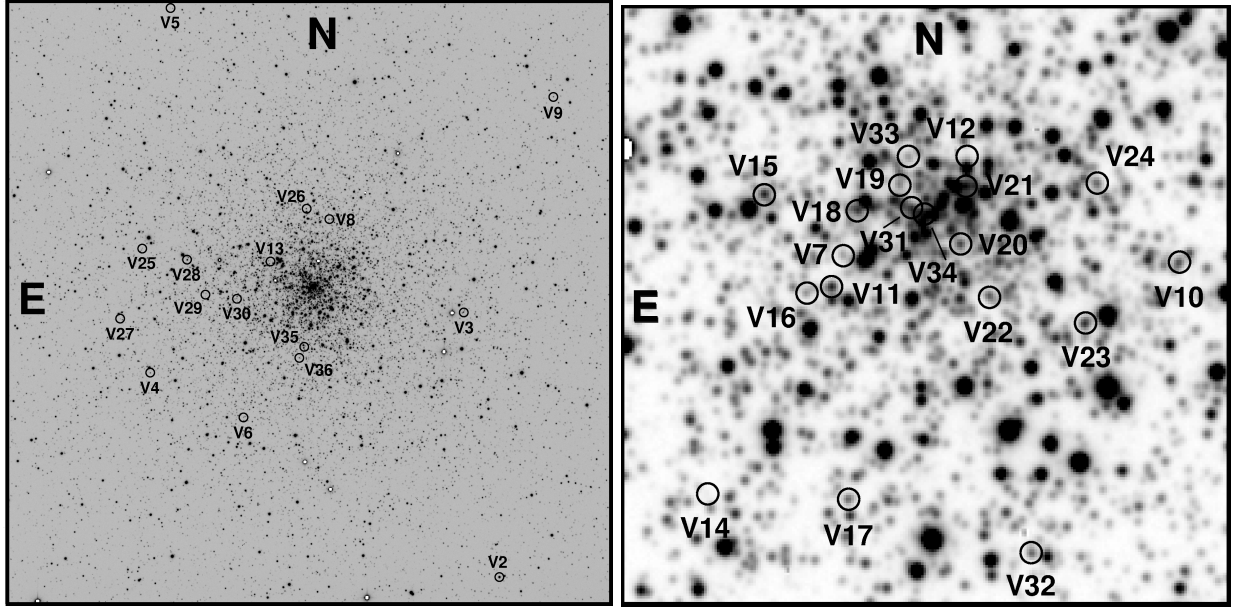


Figure 4: Identification charts for the variables in NGC 6397. *Left*, the periphery of the cluster ( $15' \times 15'$ ). *Right*, the cluster core ( $1.7' \times 1.7'$ ). Only star V1 is outside the larger field.

Table 3: Data on the variable stars of NGC 6397 reported in this work

Variable Id.	Variable Type	$\langle V \rangle^a$	$\langle I \rangle^a$	$A_V$	$A_I$	$P$	HJD <sub>max</sub> +245 0000.
		[mag]	[mag]				
V3	RRab	16.176	15.526	1.222	0.895	0.494748	8257.9189
V4	EW	16.537	15.390	0.667	0.585	0.422742	8258.8602
V5	E	18.853	16.167	1.057	0.681	0.27 <sup>c</sup>	8297.7744
V7	EW	17.657	16.694	0.905	0.836	0.2699 <sup>c</sup>	8257.8506
V8	EW	16.414	15.713	0.421	0.431	0.271240	7963.7078
V10	SX Phe	15.907 <sup>b</sup>	15.375 <sup>b</sup>	0.070	...	0.030030	7908.8962
V11	SX Phe	15.340	14.794	0.053	0.035	0.038262	8033.5452
V15	SX Phe	15.525 <sup>b</sup>	14.990 <sup>b</sup>	0.070	...	0.025240	8258.8130
V16	ELL	16.767	15.741	0.123	0.149	1.489390	8257.8884
V18	E	15.701 <sup>b</sup>	15.042 <sup>b</sup>	0.218	0.167	0.7867 <sup>c</sup>	8297.6893
V20	$\gamma$ Dor?	15.863 <sup>b</sup>	15.275 <sup>b</sup>	...	...	0.8612 <sup>c</sup>	8033.5452
V21	SX Phe	15.634	14.828	0.363	0.114	0.038961	7984.6207
V22	RRd	16.059	15.472	0.184	0.123	0.46497 0.30669	8258.7534
V23	SX Phe	15.523	14.961 <sup>b</sup>	0.081	...	0.038005	8033.5091
V24	$\gamma$ Dor?	16.174 <sup>b</sup>	15.316 <sup>b</sup>	0.123	...	0.4572 <sup>c</sup>	8033.5398
V25	?	17.987 <sup>b</sup>	16.566 <sup>b</sup>	0.190	...	1.2306 <sup>c</sup>	7998.5528

**Notes.**

<sup>a</sup>Intensity-weighted mean.

<sup>b</sup>Magnitude-weighted mean ( $\bar{V}$ ,  $\bar{I}$ ).

<sup>c</sup>CVSGC (Clement et al., 2001).

Table 4: Time-series  $V$  and  $I$  photometry for the variables in our field of view

Variable Id.	Filter	HJD [d]	$m_{\text{std}}$ [mag]	$m_{\text{ins}}$ [mag]	$\sigma_m$ [mag]
V2	$V$	2458297.56732	13.249	14.943	0.004
V2	$V$	2458297.57256	13.242	14.937	0.005
⋮	⋮	⋮	⋮	⋮	⋮
V2	$I$	2458297.58010	9.556	10.820	0.002
V2	$I$	2458297.58886	9.552	10.816	0.002
⋮	⋮	⋮	⋮	⋮	⋮
V3	$V$	2457908.85026	16.365	18.750	0.006
V3	$V$	2457908.85498	16.377	18.762	0.012
⋮	⋮	⋮	⋮	⋮	⋮
V3	$I$	2457908.84190	15.620	18.825	0.012
V3	$I$	2457908.84429	15.626	18.831	0.012
⋮	⋮	⋮	⋮	⋮	⋮

**Notes.** The columns  $m_{\text{std}}$  and  $m_{\text{ins}}$  are the standard and instrumental magnitudes, and  $\sigma_m$  is the error (the same) for both. This is an excerpt from the full table, which is available only with the electronic version of the article.

Kaluzny & Thompson (2003) discussed the possibility of V22 being a pulsating multiperiodic variable related to  $\gamma$  Doradus stars, Kaluzny et al. (2006) classified it as an RRd, with  $P_0 = 0.52$  d and  $P_1 = 0.344$  d ( $P_1/P_0 = 0.66$ ). In our analysis we found that a period  $P_0 = 0.46497$  d produces the light curve shown in Fig. 5; there is, however, evidence of a second period  $P_1$  of 0.30669 d, with which we also derive a ratio  $P_1/P_0 = 0.66$ . Both periods are listed in Table 3.

#### 4.2. SX *Phoenicis* stars

**V10.** With V11, this star was originally identified as an SX Phe variable by Kaluzny (1997). A low amplitude modulation with a periodicity of about 0.287 d is evident in the data from Las Campanas. On top of this, clear short-period variations with a period of 0.030 d are detected. This period agrees with that reported in the CVSGC (0.0308 d). An amplitude modulation of the short period variations is explained by the presence of a secondary frequency of period 0.03378 d, which is likely a non-radial mode. A model built with the said three periods is shown in Fig. 6.

**V11.** Clear monoperoiodic variations are observed in the light curves (Figs. 5 and 6), phased with a period of 0.038262 d (Kaluzny et al., 2006).

**V15.** Identified as an SX Phe variable by Kaluzny & Thompson (2003), with V21 and 23; all

of them are in the blue straggler region of the CMD. The small variations in brightness are displayed in Fig. 6. The two periods 0.02524 d and 0.02200 d represent rather well the data periodicity and the amplitude modulations. This is a very short period for an SX Phe variable. Kaluzny & Thompson (2003) found for V15 a period of 0.0215 d and discussed the possibility that it is a pulsating hot dwarf rather than an SX Phe.

**V21.** Mild variations in the  $V$ -band are seen in this SX Phe star which are properly folded with a period  $P = 0.038961$  d (see Fig. 5). This period represents well the periodic behaviour of the variations, but some mean magnitude modulations are also seen in Fig. 6, which may be due to a secondary periodicity not detected in our data.

**V23.** Small-amplitude variations are clear in this SX Phe star, showing a periodicity of 0.03805 d (Fig. 6).

#### 4.3. $\gamma$ Doradus stars?

In the CMD (Fig. 3), V20 and V24 are found among the blue straggler stars and in the main sequence near the turnoff point, respectively. Light variations of these two stars were reported by Kaluzny et al. (2006), giving periods of 0.8612 and 0.4572 d. These rather long periods for a typical SX Phe star led these authors to speculate that V20

and 24 belong to a new type of Population II variables, counterpart of the Population I  $\gamma$  Doradus class, i.e., nonradially oscillating stars locate near the intersection of the red edge of the classical instability strip and the main sequence.

**V20.** Due to seeing conditions and faintness of the star, it could not be measured in Bosque Alegre images, although it was observed at Las Campanas—albeit only five hours. The Swope light curve is in Fig. 5. A mild variation consistent with the period 0.8612 d is clearly seen, consistent with the variability and period of Kaluzny et al. (2006).

**V24.** Like V23, it presents small-amplitude variations of the SX Phe type. Our data are not properly phased with the period 0.4572 d reported by Kaluzny et al. (2006), but the combination of this value and the SX Phe-like, short-period of 0.02754 d produce the rather good representation shown in Figs. 5 and 6. In the cluster CMD (Fig. 3), the star is towards the red edge of the main sequence which, together with its proper motion, make clear that V24 does not belong to the cluster. There is a star of similar brightness at  $0.7''$  towards the NE, *Gaia* source 5921748251704160512 (cf. Fig. 1 of Kaluzny & Thompson 2003). Star V24, on the other hand, is not a *Gaia* DR2 source.

#### 4.4. Eclipsing Binaries and Ellipsoidal Variables

**V4, V7, V8.** Neat eclipses are observed for these three contact binaries or EW-type stars; the periods are 0.42274 d, 0.2699 d, and 0.27124 d, respectively. Star V7, discovered and identified as an W UMa binary by Kaluzny (1997), is not detected in our Bosque Alegre observations. Our (Las Campanas) period for V7 coincides with Kaluzny & Thompson’s (2003). In § 5 we present and discuss a modelling of these light curves.

**V5.** Its Swope light curve in *I* shows clear eclipses; the one in *V*, however, is much noisier (Fig. 5). They were phased with the period given in the CVSGC,  $P = 0.27$  d. The star is too red to appear in our CMD. An analysis of the light curves of this binary is presented in § 5.

**V6, V9, V14.** No variations were detected in our one-night data from Las Campanas for V6 and V14. On the other hand, the Swope light curve of the eclipsing binary V9 is fairly incomplete (Fig. 5) and therefore was not analysed. Nevertheless, the three stars are included in the CMD.

**V16.** This ellipsoidal variable is the optical component of the millisecond pulsar J1740–5340—

see discussion in Kaluzny & Thompson (2003) and Kaluzny et al. (2008). In Fig. 5 our light curve has been folded with the period listed by Kaluzny et al. (2006), i.e., 1.35406 d.

**V17.** This star is listed as a probable elliptical variable in the CVSGC. In our data, however, we did not detect any variations. It appears near the cluster turnoff.

**V18.** This eclipsing variable is a cluster blue straggler. Kaluzny & Thompson (2003) reported an unusual light curve (see their Fig. 10); they propose that it is a detached or semidetached system composed of stars with very similar surface brightness, rather than a contact binary. Our light curves have been phased with  $P = 0.78669$  (Kaluzny et al., 2006).

**V19.** No variations are noticed in our data. We therefore cannot confirm its reported variable nature, which appears to be of rather small amplitude (cf. Fig. 8 of Kaluzny & Thompson 2003).

#### 4.5. Cataclismic Variables

**V12, V13, V33, V34.** These stars were identified by Kaluzny et al. (2006) with the cataclismic variables CV1, CV6, CV2, and CV3 of Grindlay et al. (2001), respectively. Although they are rather faint for the precision of our photometry, or are blended with a brighter neighbour (V12), we were nevertheless able to detect and measure stars V13, V33, and V34, and include them in the CMD. However, we could not find any variations. The mild, long term or sporadic variations given by Kaluzny et al. (2006)—their Fig. 3—rather explain the lack of variations in our data.

#### 4.6. Others

**V2.** According to the CVSGC, this is a long-period (39.5977 d) variable of possibly RV Tau type. We covered it during only one night at Las Campanas; no variations were observed in its light curves, from which we estimated  $\langle V \rangle = 13.25$  and  $\langle I \rangle = 9.55$ . Its colour is too red to be represented in our CMD.

**V25.** The light curve (Fig. 5) was phased with a period of 1.2306 d (Kaluzny et al., 2006). The slight variations are not conclusive as to how classify this star.

**V28.** We could not phase properly the light curve of this rather bright ( $V \approx 15.2$  mag) star with the period 25.997 d suggested by Kaluzny et al. (2006). A plot of *V* vs. HJD (Fig. 5) shows clear

variations, and one full cycle suggests a much longer period of  $P = 97.78$  days. This new period is not rigid but is rather a characteristic time of variation, as stochastic variations are hinted by our data. The star is very red and is outside the CMD limits of Fig. 3. It was classified by Kaluzny et al. (2006) as a pulsating star, but could in fact be a spotted variable.

#### 4.7. Variables not detected

**V26, 27, 29–32, 35–36.** We were not able to detect variations using published periods or after searching for them with the string-length method. They are nevertheless represented in our CMD, with the exception of V35, which is too faint and too near a bright star.

### 5. Modelling contact binaries in NGC 6397

Figure 5 shows the  $V$ ,  $I$  light curves of the eclipsing binaries V4, V5, V7, and V8, among other stars. They evidently have morphologies typical of semidetached and contact binaries. To model the systems, we used the code BINAROCHE (Lázaro et al., 2009), which simultaneously fits both the  $V$  and  $I$  light curves.

The BINAROCHE model takes into account the deformation of the stars, in the Roche model geometry, and the inhomogeneous temperature distribution over the stellar surfaces, considering gravity darkening and heating effects. The gravity darkening exponents can be declared free parameters, but the standard values— $\beta = 0.25$  for a star with a radiative envelope, and  $\beta = 0.08$  if the star has a convective envelope—usually produce satisfactory fits. The code adopts  $T \propto g^\beta$ , with  $T$  and  $g$  being the local effective temperature and surface gravity, respectively. The filling factor  $S_i$  of each star, which is also a free parameter of the model, is defined as the ratio between its polar radius ( $r_p$ ) and the polar radius of its critical Roche lobe ( $R_p$ ):  $S_i = (r_p/R_p)_i$ ,  $i = 1, 2$ . The mass of the primary component—in solar mass units—and the mass ratio  $q = M_2/M_1$  are parameters of the model, since the stellar surface fluxes depend on  $T_{\text{eff}}$ ,  $\log g$ , and  $[\text{Fe}/\text{H}]$ . The code adopts stellar atmospheres fluxes from the BaSel library (Lejeune et al., 1998). Expressing the masses of the binary components in solar masses allows the derivation of the distance to the system in parsecs.

The analysis starts assuming the binaries are members of NGC 6397, i.e., they have the cluster’s

metallicity and interstellar extinction. The adoption of a  $E(B - V)$  value, and the relative contribution of the primary component to the total flux in  $V$  and  $I$ , a result of the light curves fits, allows us to obtain the intrinsic colour  $(V - I)_0$  of the primary star from the observed colour of the binary at the maximum. Then, the effective temperature  $T_{\text{eff},1}$  of the primary is estimated from the calibrations  $(V - I)_0$  vs.  $T_{\text{eff}}$  of Huang et al. (2015) if  $-0.8 \leq [\text{Fe}/\text{H}] \leq +0.3$ , or Casagrande et al. (2010) when  $[\text{Fe}/\text{H}] = -2.0$ .

To estimate the mass of the primary component, we adopted the relation of Torres et al. (2010) for stars in detached, non-interacting binary systems with accurately measured masses and radii. They give polynomial fits for  $\log M(M_\odot)$  and  $\log R(R_\odot)$ , in terms of  $T_{\text{eff}}$ ,  $\log g$ , and  $[\text{Fe}/\text{H}]$ . Unfortunately, these relations do not include systems with metallicity as low as  $-2.0$  dex, i.e., that adopted for NGC 6397, which introduces an additional uncertainty. The mass of the secondary star is derived from the free parameter  $q = M_2/M_1$ . Since the relative flux of the primary and  $\log g_1$  are results of the model, a few iterations are necessary to reach stable values of  $M_1$  and  $T_{\text{eff},1}$ .

Next we discuss the individual systems.

**V4.** Assuming the star to be a cluster member, with  $E(B - V) = 0.19$  and  $[\text{Fe}/\text{H}] = -2.0$ , we obtained  $T_{\text{eff},1} \approx 5200$  K and  $M_1 \approx 0.59M_\odot$ . But with these parameters, the calculated distance to the system turns out to be  $d \approx 1290$  pc, much lower than the accepted distance of NGC 6397 (see § 6). We therefore considered another solution, supposing that the binary is a field star of solar metallicity, i.e., with  $[\text{Fe}/\text{H}] = 0.0$ . Adopting a reasonable guess of  $E(B - V) = 0.10$ , we recomputed the binary parameters, which are listed in Table 5, while the observed and model light curves are shown in Fig. 7. The filling factors  $S_1$  and  $S_2$  indicate that V4 is a semidetached system, with a secondary oversized component filling its Roche lobe. Even considering the uncertainty in  $E(B - V)$ , from the derived distance it seems very likely that V4 is not a cluster member.

**V5.** Our light curve in  $V$  is rather faint and noisy, but the colour  $(V - I)$  out of eclipse indicates that it is a rather red object. Again, starting with the assumption that it is a member of NGC 6397, adopting  $E(B - V) = 0.19$  and  $[\text{Fe}/\text{H}] = -2.0$ , we derived parameters corresponding to a very low mass system, with a primary of  $M_1 \approx 0.30 M_\odot$  and  $T_{\text{eff},1} \approx 3700$  K, and a distance  $d \approx 550$  pc; this dis-

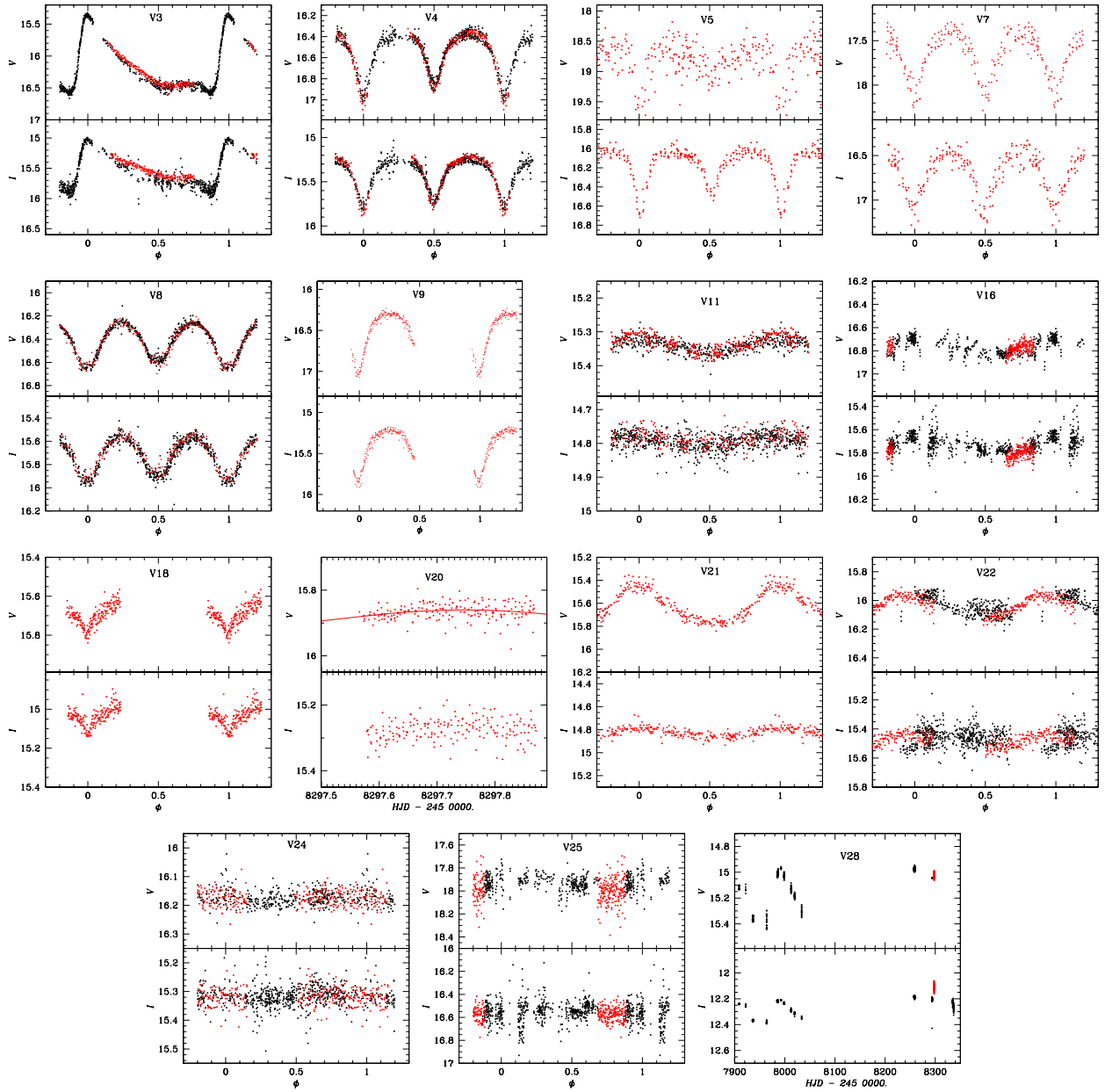


Figure 5: Light curves in  $VI$  of some variables in the field of NGC 6397. Black and red symbols stand for Bosque Alegre and Las Campanas observations, respectively. Note that V20 and V28 are not phased but plotted vs. HJD; the solid curve in V20 is the portion of a  $P = 0.8612$  d model.

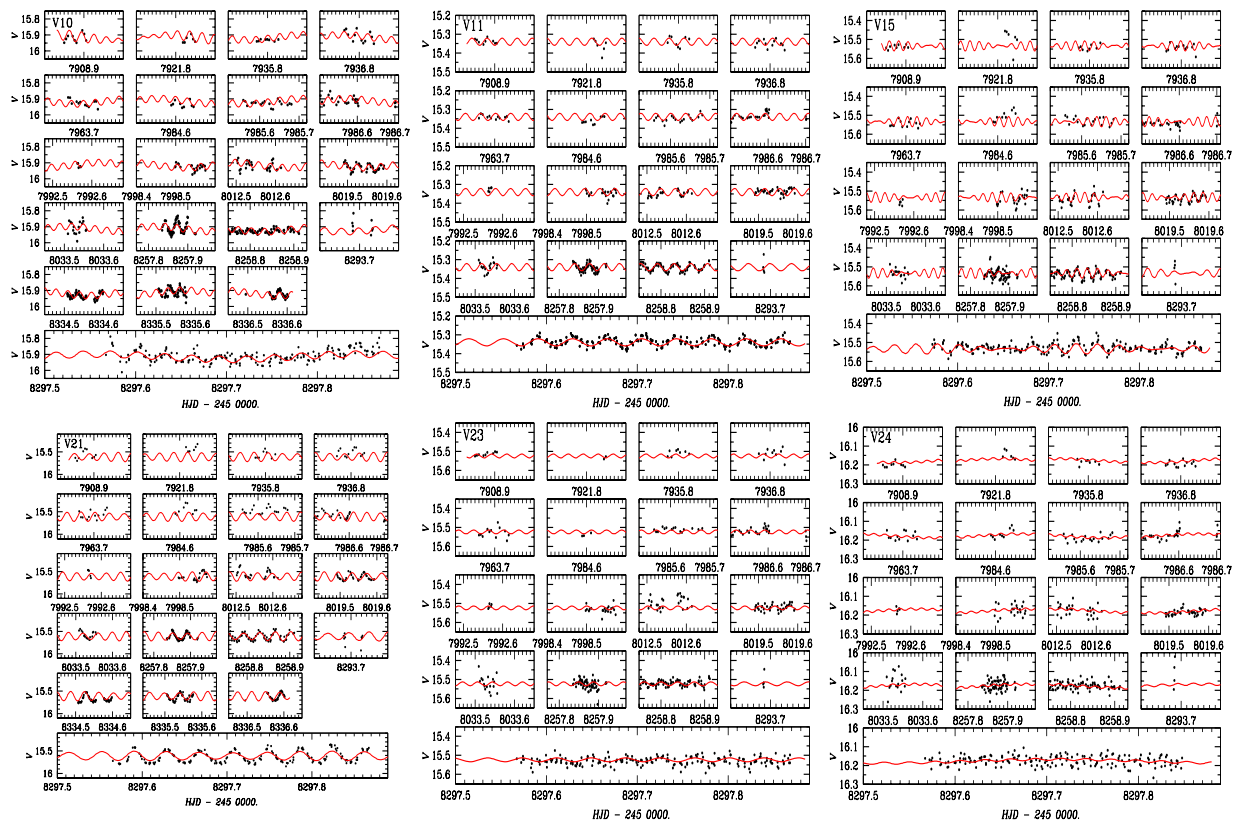


Figure 6: Light curves in  $V$  of six SX Phoenicis stars in the field of NGC 6397. The long boxes contain  $\sim 7.5$  hours of Swope data.

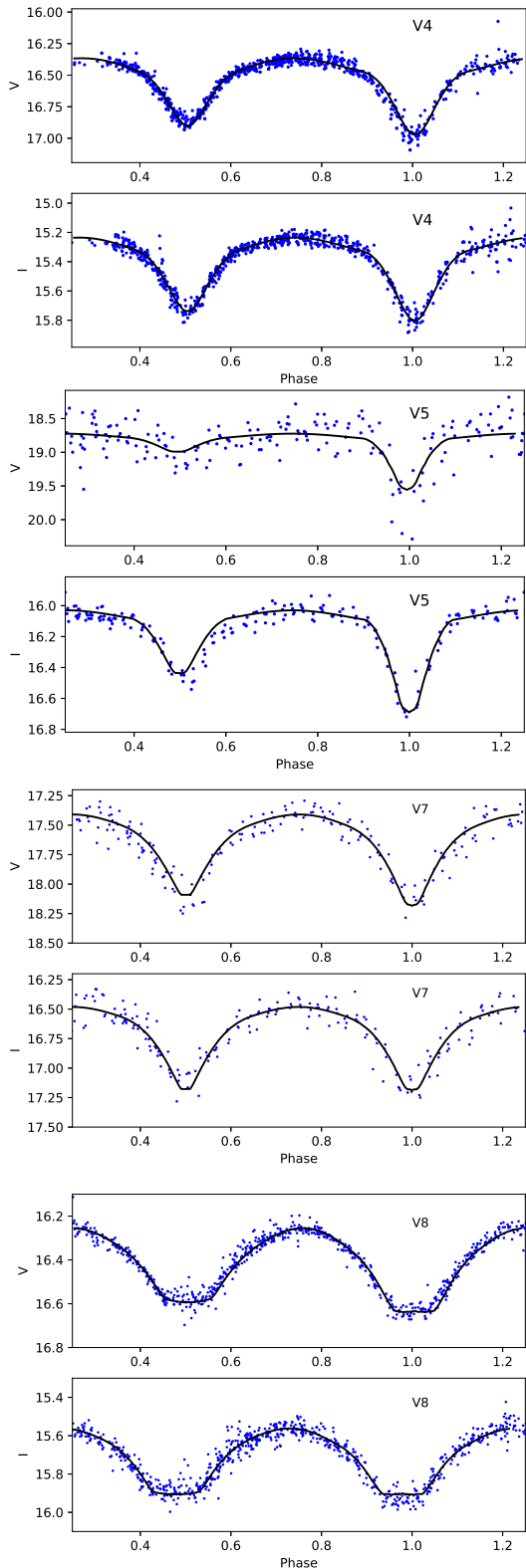


Figure 7: Light curves and fits of four eclipsing binaries in NGC 6397. The parameters of the models are in Table 5.

cards it as a member of the cluster. We repeated the process considering the binary as a field star with solar metallicity and  $E(B - V) = 0.05$ . The new results are in Table 5, and the observed and model light curves are shown in Fig. 7. The filling factors of the model suggest a detached binary. The right side of the secondary eclipse in  $I$  looks depressed relative to the model, but due to the low quality of the light curves we did not attempt to reproduce it. Like V4, it seems quite sure that V5 is also a field binary.

**V7.** The light curves show the rounded morphology typical of contact systems, but the depths of the eclipses are not well defined due to dispersion in the data. As before, we adopted  $E(B - V) = 0.19$  and  $[\text{Fe}/\text{H}] = -2.0$ . The observed and model light curves are shown in Fig. 7, and the parameters from the light curves fits are in Table 5. The filling factors of both components indicate that V7 is a contact system, and the resulting distance of  $\approx 2.6$  kpc is consistent with the assumed membership to NGC 6397.

**V8.** The light curves (Fig. 7) present a rounded morphology with flat eclipses. The parameters derived from the modelling are in Table 5, assuming that the binary belongs to the cluster. The filling factors of both components indicate that V8 is a contact system with a low mass ratio. The distance ( $\approx 2.3$  kpc) makes V8 a likely cluster member.

The binary parameters of Table 5 are presented without error bars, as the unknown systematic uncertainties involved—photometry, adopted reddening and metallicity, model atmosphere fluxes and limb darkening, adopted relations for  $T_{\text{eff},1}$  and  $M_1$ —make pointless any statistical estimation of errors. We can nevertheless consider, for example, the light curve of V8. By decreasing the observed  $(V - I)$  at maxima in 0.02 mag we obtain  $M_1 \approx 0.96M_{\odot}$ ,  $T_{\text{eff},1} \approx 7600$  K, and  $d \approx 2480$  pc. We can therefore expect that uncertainties of the order of  $\delta M_1 \approx 0.03M_{\odot}$ ,  $\delta T_{\text{eff},1} \approx 200$  K, and  $\delta d \approx 150$  pc would be rather conservative.

Additionally, we can compare the distances in Table 5 with those derived by other independent methods involving binaries. For that purpose we adopted the period-luminosity (P-L) relations of Rucinski & Duerbeck (1997) and Rucinski (2000) for W UMa binaries with Hipparcos parallaxes and for W UMa systems in globular clusters, respectively. It must be pointed out that, as V4 and V5 are a semidetached and a detached system in our solutions, using W UMa P-L relations is not entirely appropri-

ate; even so, we carried out the comparison with them as well. The metallicities used in the P-L relation of Rucinski & Duerbeck (1997) are those in Table 5. The distances obtained from the P-L relations in the bands  $V, I$  are listed in Table 6. We see that for the two W UMa systems, V7 and V8, the distances expected from the mean P-L relations are in fairly good agreement with our estimations in Table 5 and in § 6, and therefore with the standard distance of NGC 6397. On the other hand, even if they are not contact systems, V4 and V5 seem to be much nearer than the cluster.

## 6. Distance to the cluster

### 6.1. From the SX Phoenicis P-L relation

The distance to the cluster can be estimated using the Period-Luminosity (P-L) relation for its SX Phe stars. The variables V10, V11, V15, V21, and V23 are, given their proper motions in *Gaia* DR2 and positions in the CMD, very convincing SX Phe members of the system. For the calculations we employed three independent calibrations of the P-L relation, namely Poretti et al. (2008) (*long-dash*), Arellano Ferro et al. (2011) (*solid*), and Cohen & Sarajedini (2012) (*short-dash*), as shown in Fig. 8, for the fundamental (*black*), first overtone (*blue*), and second overtone (*lilac*) modes, respectively. The positioning of the first and second overtone loci was done assuming the ratios between the periods  $P_1/P_0 = 0.783$  and  $P_2/P_0 = 0.571$  (Jeon et al., 2003, 2004). It is rather clear from their distribution on the P-L plane that V10, V11, and V21 are fundamental pulsators, while the main periods in V23 and V15 correspond to the first and second overtone, respectively. Assuming these modes, and using the three calibrations for each mode, we ended up with three distance determinations for each variable—all very similar—that yield a grand average of  $2.24 \pm 0.13$  kpc. This result compares very well with the distance of 2.3 kpc in Harris (1996), and with the recent measurement by Brown et al. (2018), based on WFC3@HST geometrical parallaxes, of  $2.39 \pm 0.10$  kpc.

### 6.2. From HB and isochrones fitting

In § 3.3 we showed that a proper matching of the Victoria isochrones to the star distribution in the CMD (Fig. 3) results by adopting a reddening  $E(B - V) = 0.19$  and a distance of 2.5 kpc, in good agreement with the value obtained using the SX Phoenicis variables in § 6.1.

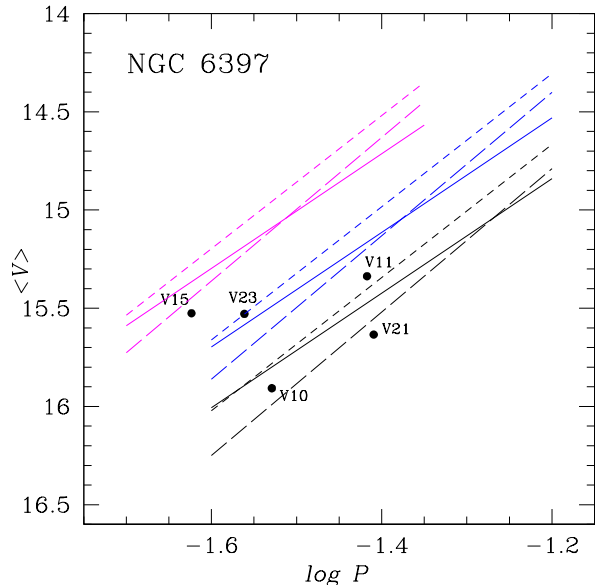


Figure 8: Period-Luminosity relations for SX Phe stars: Poretti et al. (2008) (*long-dash*), Arellano Ferro et al. (2011) (*solid*), and Cohen & Sarajedini (2012) (*short-dash*), for the fundamental (*black*), first overtone (*blue*), and second overtone (*lilac*) modes.

### 6.3. From the modelling of eclipsing binaries

As described in § 5, eclipsing binaries V7 and V8 are likely cluster members; their distances, derived from the modelling of the light curves and employing P-L relations for W UMa stars, are between 2.35 and 2.6 kpc, again consistent with the results in §§ 6.1–6.2.

## 7. The structure of the horizontal branch

We now want to draw attention to the similarity between the CMD of NGC 6397 (Fig. 3) and that of NGC 6254 (M10, see Fig. 6 of Arellano Ferro et al. 2020). In particular, the structure of the HB is worth examining. Both clusters display a well-developed blue tail and a virtually non-existent horizontal region, with the consequent absence of RR Lyrae stars, with the sole exception of the RRc V22 in M10. The likeness extends to the age ( $\approx 13$  Gyr, as suggested by the turnoff isochrone fitting).

As we did for M10, we modelled the HB of NGC 6397 with the evolution code, parametrization, and prescription of the RGB mass-loss (a modified Reimers law with  $\eta = 0.8 \times 10^{-13}$ ) of Schröder & Cuntz (2005). The code was originally developed



Table 5: Parameters derived from modelling with BINAROCHE the  $V$ ,  $I$  light curves of close binaries in NGC 6397

Variable	[Fe/H] <sup>a</sup>	$E(B - V)^a$	$M_1$ [ $M_\odot$ ]	$R_1$ [ $R_\odot$ ]	$T_{\text{eff},1}$ [K]	$S_1$	$M_2/M_1$	$R_2$ [ $R_\odot$ ]	$T_{\text{eff},2}$ [K]	$S_2$	$i$ [deg]	$d^b$ [pc]
V4	0.00	0.10	0.82	0.76	5000	0.74	1.00	1.05	4875	1.00	80.5	1525
V5	0.00	0.05	0.42	0.48	3475	0.75	0.46	0.41	3135	0.90	88.0	490
V7	-2.00	0.19	0.68	0.75	5950	1.00	0.75	0.66	5615	1.00	87.5	2495
V8	-2.00	0.19	0.94	0.90	7420	1.00	0.32	0.54	5886	1.00	87.3	2350

**Notes.**

<sup>a</sup>Adopted values for the model.

<sup>b</sup>Mean value of distance from  $V$  and  $I$ .

Table 6: Distances in parsecs derived from P-L relations for W UMa binaries in NGC 6397

Variable	$d_V$ (RD97)	$d_I$ (RD97)	$d_V$ (R00)
V4	1630	1755	1627
V5	231	312	230
V7	2354	2383	2622
V8	2070	2020	2305

**Notes.** The values  $d_V$  and  $d_I$  are distances derived from light curves in  $V$  and  $I$ . RD97: Rucinski & Duerbeck (1997); R00: Rucinski (2000).

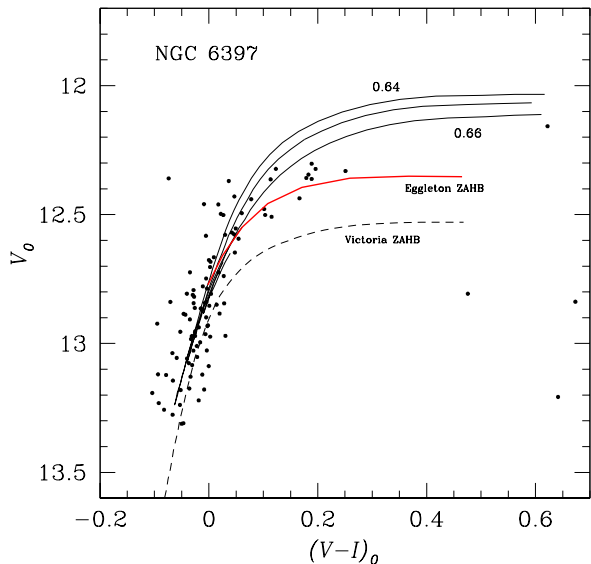


Figure 9: Enlargement of the HB region in the CMD (Fig. 3), showing in detail the matching to the observations by the Eggleton evolutionary tracks and ZAHB, and by the Victoria ZAHB. Discussion is in § 7.

by Peter Eggleton (1971; 1972; 1973), and further improved and tested by Pols et al. (1997, 1998) and Schröder et al. (1997).

The very blue end of the HB of NGC 6397 suggests rather thin hydrogen shell masses, consistent with the best-match HB models plotted in the CMD (Fig. 3, or the magnification in Fig. 9), of total mass between 0.64 and 0.66  $M_\odot$ . This values are similar to those we found for M10 (see Fig. 8 of Arellano Ferro et al. 2020). In Fig. 9 we added the theoretical ZAHB line derived from our Eggleton (Cambridge) code, and compared it to a standard ZAHB of the well-established Victoria models, for [Fe/H] = -2.0, [ $\alpha$ /Fe] = +0.4, and  $Y = 0.25$  (VandenBerg et al., 2014). Note that HB stars evolve upwards of their ZAHB starting points, and such a line should, therefore, ideally demarcate a lower boundary to the distribution of observed HB stars in the CMD. While our ZAHB line does so, the Victoria ZAHB appears to leave a gap, indicating that the respective models are less luminous than the observed HB stars of NGC 6397 by almost 0.2 mag. This seems to be at odds with the fact that both codes (Eggleton and Victoria) are mutually consistent in their results. They share the Eggleton approach of an adaptive, non-lagrangian mesh, which places more mesh points in regions with large temperature and pressure gradients. However, the standard Victoria ZAHB uses He-core masses of approximately 0.49  $M_\odot$ , as D. VandenBerg pointed out in a private communication. The models we computed for M10 and this cluster, by contrast, reach a slightly higher He-core mass of 0.51  $M_\odot$ . This is a small difference in mass (about 4%) but, by virtue of the mass-luminosity relation—much like in main-sequence stars—there is a change in brightness which is fully responsible for the afore-

mentioned difference of 0.2 mag.

It is pertinent to note that we systematically stop our tip-*RGB* evolution models just before the He-flash, when the already slowly burning helium exceeds a luminosity of  $10 L_{\odot}$  (Arceo-Díaz et al., 2015). Beyond this point, the exponential growth of the He-burning leads to the He-flash and to a non-equilibrium transition towards the ZAHB, which most evolution codes do not cover. There is, in other words, a sort of final “He-simmering” time at the tip of the *RGB*, especially when the hydrogen shell around the core has been much reduced by mass loss; this should be expected, e.g., in old globular clusters, hence causing the very blue HB stars in M10 and NGC 6397. This final “tip-*RGB* time” makes the helium cores of our models a little more massive than those of the conventional Victoria ZAHB models.

## 8. Summary and conclusions

We have presented the photometric analysis of a new time-series of *VI* CCD images of the post-core-collapse globular cluster NGC 6397. The data reduction and the photometry were carried out with the Differential Image Analysis (DIA) procedure. In an already extensive series of papers by our group (see, e.g., AF17), we have shown that DIA is a powerful tool to generate massive numbers of good-quality light curves for all the objects present in a specific sky field, with particular interest in the light curves of variable stars. Unfortunately, NGC 6397 does not harbour RR Lyrae stars, which are proper for a Fourier light curve decomposition analysis; however, we had at our disposal another types of variables and diverse tools to take advantage toward the determination of the cluster distance and metallicity.

First, we cleaned the CMD making use of the powerful *Gaia* DR2 astrometric solution and the BIRCH algorithm, selecting the most likely members (almost 13,000 stars in Las Campanas data, § 3.1). After a differential dereddening of the CMD (§ 3.2), isochrones for 13.0–13.5 Gyr and  $[\text{Fe}/\text{H}] = -2.0$  from VandenBerg et al. (2014) were then matched to the main sequence, turnoff, and *RGB* (Fig. 3, *right*). The matching is good for a distance of 2.5 kpc and a mean reddening  $E(B - V) = 0.19$ . An independent method for deriving the cluster distance involves the Period-Luminosity relation for the SX Phoenicis variables present among its blue

straggler population (§ 6.1). Using three different P-L relations for five SX Phe stars (V10, V11, V15, V21, and V23), we obtained a mean value of  $2.24 \pm 0.13$  kpc. Yet another distance determinations come from the cluster’s eclipsing binaries V4, V5, V7, and V8. A first method uses the modelling of their light curves with the BINAROCHE code (§ 5); it turns out that, while V4 and V5 are a semidetached and a detached system fairly nearer than the cluster, V7 and V8 are contact binaries at 2.6 and 2.3 kpc, thus being likely cluster members (Table 5). These results are furthermore confirmed by using a P-L relation for W UMa binaries (Table 6).

The blue horizontal branch of NGC 6397 is similar to that of M10 which, however, harbours just one RR Lyrae (Arellano Ferro et al., 2020), while NGC 6397 has none. The models of 0.64–0.66  $M_{\odot}$  with mass loss at the *RGB* (Schröder & Cuntz, 2005), located at the distance and reddening suggested by the isochrones fitting to the TO and *RGB*, provide a good matching of the HB stars. Comparing with M10, this means that a minor range of mass loss at the *RGB*—i.e., a minor range of mass of the remaining envelopes above de He-core—represents better the observations. By contrast, in M10 that range is wider, 0.56–0.62  $M_{\odot}$ ; it must be pointed out, however, that the HB of M10 is richer and extends longer towards faint magnitudes than that of NGC 6397. The difference of mass loss during the *RGB* stage might be ascribed to magnetic fields in the stars’ chromospheres that somehow hinder the normal losses (Arellano Ferro et al., 2020).

## Acknowledgements

AAF acknowledges the support from DGAPA-UNAM grant through project IG100620. It is a pleasure to thank Dr. Don A. VandenBerg for the use of his model interpolation software and for an instructive discussion on horizontal branch models.

## References

- Alonso-García, J., Mateo, M., Sen, B., Banerjee, M., Cateilan, M., Minniti, D., & von Braun, K. (2012). *AJ*, *143*, 70.
- Arceo-Díaz, S., Schröder, K. P., Zuber, K., & Jack, D. (2015). *RMxAA*, *51*, 151.
- Arellano Ferro, A., Bramich, D. M., & Giridhar, S. (2017). *RMxAA*, *53*, 121. (AF17).

- Arellano Ferro, A., Figuera Jaimes, R., Giridhar, S., Bramich, D. M., Hernández Santisteban, J. V., & Kuppuswamy, K. (2011). *MNRAS*, *416*, 2265.
- Arellano Ferro, A., Yopez, M. A., Muneer, S., Bustos Fierro, I. H., Schröder, K. P., Giridhar, S., & Calderón, J. H. (2020). *MNRAS*, *499*, 4026.
- Auriere, M., Lauzeral, C., & Ortolani, S. (1990). *Nat*, *344*, 638.
- Bailey, S. I. (1902). *Annals of Harvard College Observatory*, *38*.
- Bramich, D. M. (2008). *MNRAS*, *386*, L77.
- Bramich, D. M., Figuera Jaimes, R., Giridhar, S., & Arellano Ferro, A. (2011). *MNRAS*, *413*, 1275.
- Bramich, D. M., & Freudling, W. (2012). *MNRAS*, *424*, 1584.
- Bramich, D. M., Horne, K., Albrow, M. D., Tsapras, Y., Snodgrass, C., Street, R. A., Hundertmark, M., Kains, N., Arellano Ferro, A., Figuera, J. R., & Giridhar, S. (2013). *MNRAS*, *428*, 2275.
- Brown, T. M., Casertano, S., Strader, J., Riess, A., Vandenberg, D. A., Soderblom, D. R., Kalirai, J., & Salinas, R. (2018). *ApJL*, *856*, L6.
- Bustos Fierro, I. H., & Calderón, J. H. (2019). *MNRAS*, *488*, 3024.
- Carretta, E., Bragaglia, A., Gratton, R., D’Orazi, V., & Lucatello, S. (2009). *A&A*, *508*, 695.
- Casagrande, L., Ramírez, I., Meléndez, J., Bessell, M., & Asplund, M. (2010). *A&AS*, *512*, A54.
- Clement, C. M., Muzzin, A., Dufton, Q., Ponnampalam, T., Wang, J., Burford, J., Richardson, A., Rosebery, T., Rowe, J., & Hogg, H. S. (2001). *AJ*, *122*, 2587.
- Cohen, R. E., & Sarajedini, A. (2012). *MNRAS*, *419*, 342.
- Cohn, H. N., Lugger, P. M., Couch, S. M., Anderson, J., Cool, A. M., van den Berg, M., Bogdanov, S., Heinke, C. O., & Grindlay, J. E. (2010). *ApJ*, *722*, 20.
- Correnti, M., Gennaro, M., Kalirai, J. S., Cohen, R. E., & Brown, T. M. (2018). *ApJ*, *864*, 147.
- Djorgovski, S., & King, I. R. (1986). *ApJL*, *305*, L61.
- Dworetsky, M. M. (1983). *MNRAS*, *203*, 917.
- Eggleton, P. P. (1971). *MNRAS*, *151*, 351.
- Eggleton, P. P. (1972). *MNRAS*, *156*, 361.
- Eggleton, P. P. (1973). *MNRAS*, *163*, 279.
- Gratton, R. G., Bragaglia, A., Carretta, E., Clementini, G., Desidera, S., Grundahl, F., & Lucatello, S. (2003). *A&A*, *408*, 529.
- Grindlay, J. E., Heinke, C. O., Edmonds, P. D., Murray, S. S., & Cool, A. M. (2001). *ApJL*, *563*, L53.
- Harris, W. E. (1996). *AJ*, *112*, 1487.
- Huang, Y., Liu, X. W., Yuan, H. B., Xiang, M. S., Chen, B. Q., & Zhang, H. W. (2015). *MNRAS*, *454*, 2863.
- Jeon, Y.-B., Lee, M. G., Kim, S.-L., & Lee, H. (2003). *AJ*, *125*, 3165.
- Jeon, Y.-B., Lee, M. G., Kim, S.-L., & Lee, H. (2004). *AJ*, *128*, 287.
- Kaluzny, J. (1997). *A&AS*, *122*, 1.
- Kaluzny, J., & Thompson, I. B. (2003). *AJ*, *125*, 2534.
- Kaluzny, J., Thompson, I. B., Krzeminski, W., & Schwarzenberg-Czerny, A. (2006). *MNRAS*, *365*, 548.
- Kaluzny, J., Thompson, I. B., Rucinski, S. M., & Krzeminski, W. (2008). *AJ*, *136*, 400.
- Lauzeral, C., Ortolani, S., Auriere, M., & Melnick, J. (1992). *A&A*, *262*, 63.
- Lázaro, C., Arévalo, M. J., & Almenara, J. M. (2009). *NA*, *14*, 528.
- Lejeune, T., Cuisinier, F., & Buser, R. (1998). *A&AS*, *130*, 65.
- Marcano, M. P., Rivera Sandoval, L. E., Maccarone, T. J., Zhao, Y., & Heinke, C. O. (2021). *MNRAS*, *503*, L51.
- Martinazzi, E., Kepler, S. O., & Costa, J. E. S. (2017). *MNRAS*, *468*, 2816.
- Nascimbeni, V., Bedin, L. R., Piotto, G., De Marchi, F., & Rich, R. M. (2012). *A&A*, *541*, A144.
- Pols, O. R., Schröder, K.-P., Hurley, J. R., Tout, C. A., & Eggleton, P. P. (1998). *MNRAS*, *298*, 525.
- Pols, O. R., Tout, C. A., Schroder, K.-P., Eggleton, P. P., & Manners, J. (1997). *MNRAS*, *289*, 869.
- Poretti, E., Clementini, G., Held, E. V., Greco, C., Mateo, M., Dell’Arciprete, L., Rizzi, L., Gullieuszik, M., & Maio, M. (2008). *ApJ*, *685*, 947.
- Rucinski, S. M. (2000). *AJ*, *120*, 319.
- Rucinski, S. M., & Duerbeck, H. W. (1997). *PASP*, *109*, 1340.
- Samus, N. N., Kazarovets, E. V., Durevich, O. V., Kireeva, N. N., & Pastukhova, E. N. (2017). *Astronomy Reports*, *61*, 80.
- Sawyer, H. B. (1955). *J. R. Astron. Soc. Can.*, *49*, 114.
- Schlafly, E. F., & Finkbeiner, D. P. (2011). *ApJ*, *737*, 103.
- Schlegel, D. J., Finkbeiner, D. P., & Davis, M. (1998). *ApJ*, *500*, 525.
- Schröder, K.-P., & Cuntz, M. (2005). *ApJL*, *630*, L73.
- Schröder, K.-P., Pols, O. R., & Eggleton, P. P. (1997). *MNRAS*, *285*, 696.
- Shara, M. M., Hinkley, S., Zurek, D. R., Knigge, C., & Dieball, A. (2005). *AJ*, *130*, 1829.
- Stetson, P. B. (2000). *PASP*, *112*, 925.
- Torres, G., Andersen, J., & Giménez, A. (2010). *AAPR*, *18*, 67.
- Trager, S. C., King, I. R., & Djorgovski, S. (1995). *AJ*, *109*, 218.
- Vandenberg, D. A., Bergbusch, P. A., Ferguson, J. W., & Edvardsson, B. (2014). *ApJ*, *794*, 72.
- Zhang, T., Ramakrishnan, R., & Livny, M. (1996). *SIGMOD Rec.*, *25*, 103.